Scattering and propagation of terahertz pulses in random soot aggregate systems*

Li Hai-Ying(李海英)†, Wu Zhen-Sen(吴振森), Bai Lu(白 璐), and Li Zheng-Jun(李正军)

School of Physics and Optoelectronic Engineering, Xidian University, Xi'an 710071, *China*

(Received 7 August 2013; revised manuscript received 7 October 2013; published online 25 March 2014)

Scattering and propagation of terahertz pulses in random soot aggregate systems are studied by using the generalized multi-particle Mie-solution (GMM) and the pulse propagation theory. Soot aggregates are obtained by the diffusion-limited aggregation (DLA) model. For a soot aggregate in soot aggregate systems, scattering characteristics are analyzed by using the GMM. Scattering intensities versus scattering angles are given. The effects of different positions of the aggregate on the scattering intensities, scattering cross sections, extinction cross sections, and absorption cross sections are computed and compared. Based on pulse propagation in random media, the transmission of terahertz pulses in random soot aggregate systems is determined by the two-frequency mutual coherence function. Numerical simulations and analysis are given for terahertz pulses (0.7956 THz).

Keywords: soot aggregate systems, terahertz pulse, scattering and propagation

PACS: 42.25.Dd, 42.68.Ay, 42.68.Mj **DOI:** 10.1088/1674-1056/23/5/054201

1. Introduction

Detection and control of unburned fuel and dust are important parts of environmental protection. In many practical situations, the effects of soot and dust particles on radio wave communication cannot be ignored completely. The scattering and propagation of an electromagnetic wave by soot and dust particles can provide meaningful results about the size and number density[1] of those particles for environmental and communication fields, and the topic has been studied widely from the ultraviolet to infrared band. However, there are few references to the characteristics of soot and dust in the terahertz band.

Generally, we define the unburned fuel and dust as soot aggregate systems, which can be considered as clusters of spherical elements and have complex structures and fractal properties. Diffusion-limited aggregation (DLA),[2] which was proposed by Witten and Sander in 1981, is used to simulate the soot aggregate systems.

Terahertz (THz) band is a generic term for waves with a spectrum between 0.1 THz and 10 THz (the corresponding wavelengths extending from 3 mm up to 30 μm). Some unique physical phenomena and features appear in this range of frequencies and this has attracted the interest of many researchers.[3,4]

Several electromagnetic scattering theories have been published regarding multisphere scattering,[5–9] for example, the discrete-dipole approximation (DDA)[5] initiated by Purcell & Pennypacker, the T-matrix method[6] developed by Waterman, the recursive aggregate interaction matrix algorithm (RAIMA)[7] provided by Chew, and the generalized Lorenz–Mie theory suggested by Gouesbet.[8] In particular, the generalized multi-particle Mie-solution (GMM) introduced by Xu[9], which is an extension of the Lorenz–Mie theory to the multi-sphere case, is generally applied to an arbitrary aggregate of spherical particles. Scattering characteristics of light by soot aggregate particles are studied in Ref. [10] by using the DDA. By using an improved GMM algorithm, we have studied the scattering of multi-sphere structures located in a plane wave/Gaussian beam.[11]

A number of important studies have reported on the propagation of plane wave and beam wave pulses in random media.[12–19] For example, Knollman[12] pointed out the theory of pulse propagation in anisotropic randomly inhomogeneous media. Ishimaru[13] developed the theory of pulse propagation in discrete random media, derived the correlation function of a wave in a random distribution of stationary and moving scatters, and reported the multiple scattering effects on coherent bandwidth and pulse distortion of a wave propagating in a random distribution of particles. Hong described the theory of plane wave pulse propagation through a random medium,[14] and considered the propagation of pulse waves of millimeter and optical waves in rain, fog, and turbulence.[15] An experimental study on picosecond pulse propagation in a diffuse medium was presented by Kuga.[16] Sreenivasiah showed an analytic solution of the beam-wave pulses propagation in random media.[17] Young gave an analytic solution for the two-frequency mutual coherence function of a Gaussian beam pulse in weak optical turbulence.[18] Liu *et al.*[19]

*Project supported by the National Natural Science Foundation of China (Grant Nos. 60971065, 61308025, and 61172031) and the Fundamental Research Funds for the Central Universities of Ministry of Education of China (Grant No. K5051207014).

†Corresponding author. E-mail: lihy@xidian.edu.cn

© 2014 Chinese Physical Society and IOP Publishing Ltd

analyzed the temporal statics of multiple scattered broadband terahertz pulses through a highly scattering medium.

For visible light and IR light, scattering by a monomer in soot clouds and transmission by soot layers have been widely discussed.[10,20,21] Meanwhile, we have investigated the same problem for THz continual waves.[22] However, little attention has been devoted to the propagation of THz pulses in random media. In this paper, we present the scattering and propagation characteristics of THz pulses in a soot aggregate system. The results of this study will be applied to the detection of soot clouds in the atmosphere.

The organization of the rest of paper is as follows. In Section 2, we briefly describe the basic theory consisting of the GMM and pulse propagation. Numerical results of scattering characteristics are presented in Section 3, where we obtain the scattering characteristics of soot aggregates by GMM. Numerical results of propagation properties are outlined in Section 4, where we give the two-frequency mutual coherence function coherence bandwidth in a soot aggregate system, and the effects of aggregate parameters. Conclusions and possible extensions are discussed in Section 5.

2. Basic theory

2.1. Generalized multi-sphere Mie-solution

As shown in Fig. 1, a multi-sphere structure of L spheres is illuminated by a plane wave. The electric field $\boldsymbol{E}_{\rm inc} = E_0(\boldsymbol{e}_x\cos\beta_{\rm p} + \boldsymbol{e}_y\sin\beta_{\rm p})\exp({\rm i}kz - {\rm i}\omega t)$. The k is the wave number of the incident beam in the surrounding medium. The ω is the circular frequency of the incident wave. The harmonic time term $\exp(-{\rm i}\omega t)$ will be suppressed.

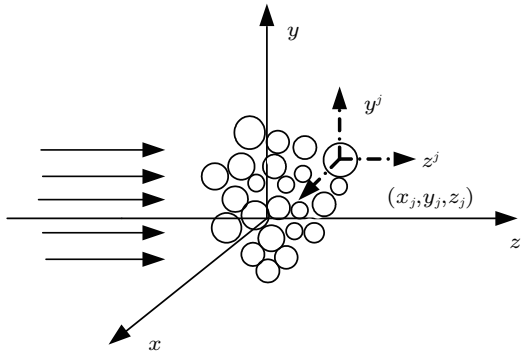


Fig. 1. A plane wave incident on an aggregate consisting of many spheres.

By using vector spherical wave functions (VSWFs), the incident wave in the primary coordinate system can be expanded as

$$\boldsymbol{E}_{\rm inc} = -\sum_{n=0}^{\infty}\sum_{m=-n}^{n}{\rm i}E_{mn}\left[q_{mn}\boldsymbol{M}_{mn}^{(1)} + p_{mn}\boldsymbol{N}_{mn}^{(1)}\right], \tag{1a}$$

$$\boldsymbol{H}_{\rm inc} = -\frac{k}{\omega\mu_0}\sum_{n=0}^{\infty}\sum_{m=-n}^{n}E_{mn}\left[p_{mn}\boldsymbol{M}_{mn}^{(1)} + q_{mn}\boldsymbol{N}_{mn}^{(1)}\right], \tag{1b}$$

where $E_{mn} = E_0{\rm i}^n(2n+1)(n-m)!/(n+m)!$, μ_0 is the permeability of the surrounding medium, $\boldsymbol{M}_{mn}^{(1)}$ and $\boldsymbol{N}_{mn}^{(1)}$ are the first kind of VSWFs.[9] The primary expansion coefficients p_{mn} and q_{mn} in Eq. (1) are given by Xu.[9]

Meanwhile, in the local coordinate system $O_j(x^j, y^j, z^j)$, the incident field, the scattered field and the internal field of the j-th sphere can also be expanded in terms of VSWFs

$$\boldsymbol{E}_{\rm inc}^{j0} = -\sum_{n=0}^{\infty}\sum_{m=-n}^{n}{\rm i}E_{mn}\Big[q_{mn}^{j0}\boldsymbol{M}_{mn}^{(1)}(r^j,\theta^j,\phi^j) + p_{mn}^{j0}\boldsymbol{N}_{mn}^{(1)}(r^j,\theta^j,\phi^j)\Big], \tag{2a}$$

$$\boldsymbol{H}_{\rm inc}^{j0} = -\frac{k}{\omega\mu_0}\sum_{n=0}^{\infty}\sum_{m=-n}^{n}E_{mn}\Big[p_{mn}^{j0}\boldsymbol{M}_{mn}^{(1)}(r^j,\theta^j,\phi^j) + q_{mn}^{j0}\boldsymbol{N}_{mn}^{(1)}(r^j,\theta^j,\phi^j)\Big], \tag{2b}$$

$$\boldsymbol{E}_{\rm s}^{j}(r^j,\theta^j,\phi^j) = \sum_{n=1}^{\infty}\sum_{m=-n}^{n}{\rm i}E_{mn}\Big[a_{mn}^{j}\boldsymbol{N}_{mn}^{(3)}(r^j,\theta^j,\phi^j) + b_{mn}^{j}\boldsymbol{M}_{mn}^{(3)}(r^j,\theta^j,\phi^j)\Big], \tag{3a}$$

$$\boldsymbol{H}_{\rm s}^{j}(r^j,\theta^j,\phi^j) = \frac{k}{\omega\mu_0}\sum_{n=1}^{\infty}\sum_{m=-n}^{n}E_{mn}\Big[b_{mn}^{j}\boldsymbol{N}_{mn}^{(3)}(r^j,\theta^j,\phi^j) + a_{mn}^{j}\boldsymbol{M}_{mn}^{(3)}(r^j,\theta^j,\phi^j)\Big], \tag{3b}$$

$$\boldsymbol{E}_{1}^{j}(r^j,\theta^j,\phi^j) = -\sum_{n=1}^{\infty}\sum_{m=-n}^{n}{\rm i}E_{mn}\Big[d_{mn}^{j}\boldsymbol{N}_{mn}^{(1)}(r^j,\theta^j,\phi^j) + c_{mn}^{j}\boldsymbol{M}_{mn}^{(1)}(r^j,\theta^j,\phi^j)\Big], \tag{4a}$$

$$\boldsymbol{H}_{1}^{j}(r^j,\theta^j,\phi^j) = -\frac{k^j}{\omega\mu^j}\sum_{n=1}^{\infty}\sum_{m=-n}^{n}E_{mn}\Big[c_{mn}^{j}\boldsymbol{N}_{mn}^{(1)}(r^j,\theta^j,\phi^j) + d_{mn}^{j}\boldsymbol{M}_{mn}^{(1)}(r^j,\theta^j,\phi^j)\Big]. \tag{4b}$$

The expansion coefficients in Eq. (2)[9] are shown as

$$p_{mn}^{j0} = \exp({\rm i}kz^j)p_{mn},\quad q_{mn}^{j0} = \exp({\rm i}kz^j)q_{mn}. \tag{5}$$

Let us translate the scattered fields of other spheres into the j-th local coordinate system, and expand them by using the first kind of VSWF. Then the real incident field of the j-th sphere can be written as

$$\begin{aligned}\boldsymbol{E}_{\rm inc}^{j} &= \boldsymbol{E}_{\rm inc}^{j0} + \sum_{l\neq j}\boldsymbol{E}_{\rm s}^{l}\\ &= -\sum_{n=1}^{\infty}\sum_{m=-n}^{n}{\rm i}E_{mn}\Big[p_{mn}^{j}\boldsymbol{N}_{mn}^{(1)}(r^j,\theta^j,\phi^j) + q_{mn}^{j}\boldsymbol{M}_{mn}^{(1)}(r^j,\theta^j,\phi^j)\Big],\end{aligned} \tag{6a}$$

$$\begin{aligned}\boldsymbol{H}_{\rm inc}^{j} &= \boldsymbol{H}_{\rm inc}^{j0} + \sum_{l\neq j}\boldsymbol{H}_{\rm s}^{l}\\ &= -\frac{k}{\omega\mu_0}\sum_{n=1}^{\infty}\sum_{m=-n}^{n}E_{mn}\Big[q_{mn}^{j}\boldsymbol{N}_{mn}^{(1)}(r^j,\theta^j,\phi^j) + p_{mn}^{j}\boldsymbol{M}_{mn}^{(1)}(r^j,\theta^j,\phi^j)\Big],\end{aligned} \tag{6b}$$

where

$$p_{mn}^{j} = p_{mn}^{j0} - \sum_{l=1(l\neq j)}^{L}\sum_{n'=1}^{\infty}\sum_{m'=-n'}^{n'} E_{m'n'}/E_{mn} \times \left[a_{m'n'}^{l}A_{m'n',mn}^{(3)}(l,j) + b_{m'n'}^{l}B_{m'n',mn}^{(3)}(l,j)\right],$$

$$q_{mn}^{j} = q_{mn}^{j0} - \sum_{l=1(l\neq j)}^{L}\sum_{n'=1}^{\infty}\sum_{m'=-n'}^{n'} E_{m'n'}/E_{mn} \times \left[a_{m'n'}^{l}B_{m'n',mn}^{(3)}(l,j) + b_{m'n'}^{l}A_{m'n',mn}^{(3)}(l,j)\right].$$

The vector transfer coefficients $A_{m'n'mn}^{(3)}(l,j)$ and $B_{m'n'mn}^{(3)}(l,j)$[9] designate the transformation of the third VSWFs in the l-th local coordinate to the first ones in the j-th local coordinate.

The continuous boundary conditions of electromagnetic fields on the surface between the air region and an arbitrary sphere in the system are

$$\boldsymbol{E}_{\rm it} + \boldsymbol{E}_{\rm st} = \boldsymbol{E}_{\rm 1t}, \quad \boldsymbol{H}_{\rm it} + \boldsymbol{H}_{\rm st} = \boldsymbol{H}_{\rm 1t}. \tag{7}$$

Substituting the tangential electric and magnetic field components at the boundary surface into Eq. (7), we obtain four linear equations. After solving these equations, the partial scattering coefficients of the j-th sphere can be obtained and shown as

$$a_{mn}^{j} = a_{n}^{j}p_{mn}^{j}, \quad b_{mn}^{j} = b_{n}^{j}q_{mn}^{j}, \tag{8}$$

where the factors a_n^j and b_n^j denote the scattering coefficients of the j-th sphere located in a plane wave incidence.

Let us repeat the similar analytical process for all spheres in the structure; the scattered field of each sphere can be obtained. The scattered field of the structure consisting of L sphere components is the sum of all partial scattered fields in the principal coordinate system. The total scattered field in the principal coordinate system can be expanded as

$$\boldsymbol{E}_{\rm s}(r,\theta,\phi) = \sum_{n=1}^{\infty}\sum_{m=-n}^{n} {\rm i}E_{mn}\left[a_{mn}\boldsymbol{N}_{mn}^{(3)}(r,\theta,\phi) + b_{mn}\boldsymbol{M}_{mn}^{(3)}(r,\theta,\phi)\right], \tag{9a}$$

$$\boldsymbol{H}_{\rm s}(r,\theta,\phi) = \frac{k}{\omega\mu_0}\sum_{n=1}^{\infty}\sum_{m=-n}^{n} E_{mn}\left[b_{mn}\boldsymbol{N}_{mn}^{(3)}(r,\theta,\phi) + a_{mn}\boldsymbol{M}_{mn}^{(3)}(r,\theta,\phi)\right]. \tag{9b}$$

By using the addition theorem of the third kind of VSWFs, the total scattering coefficients of the structure can be written as

$$a_{mn} = \sum_{l=1}^{L}\sum_{n'=1}^{\infty}\sum_{m'=-n'}^{n'} \frac{E_{m'n'}}{E_{mn}} \times \left[a_{m'n'}^{l}A_{m'n',mn}^{(1)} + b_{m'n'}^{l}B_{m'n',mn}^{(1)}\right], \tag{10a}$$

$$b_{mn} = \sum_{l=1}^{L}\sum_{n'=1}^{\infty}\sum_{m'=-n'}^{n'} \frac{E_{m'n'}}{E_{mn}} \times \left[a_{m'n'}^{l}B_{m'n',mn}^{(1)} + b_{m'n'}^{l}A_{m'n',mn}^{(1)}\right], \tag{10b}$$

where $A_{m'n'mn}^{(1)}$ and $B_{m'n'mn}^{(1)}$[9] are the vector translation coefficients, characterizing the transformation of the scattered fields from the l-th local coordinate system into the scattered field in the principal coordinate system.

2.2. Two-frequency mutual coherence function of pulse propagation

The propagation characteristics of a pulse wave in a random medium are determined by the two-frequency mutual coherence function.[13] The two-frequency mutual coherence function Γ describes the correlation between the field $u_1(\omega_1,\boldsymbol{r}_1,t_1)$ observed at a point $\boldsymbol{r}_1$ and time t_1 and the complex conjugate of the field $u_2(\omega_2,\boldsymbol{r}_2,t_2)$, and the time-harmonic factor $\exp(-{\rm i}\omega t)$ is left out. The Γ is

$$\Gamma(\omega_1,\omega_2,\boldsymbol{r}_1,\boldsymbol{r}_2,t_1,t_2) = \langle u_1(\omega_1,\boldsymbol{r}_1,t_1)u_2(\omega_2,\boldsymbol{r}_2,t_2)\rangle. \tag{11}$$

Assuming the z axis along the direction of wave propagation, and the position vector $\boldsymbol{r} = \boldsymbol{\rho} + z\boldsymbol{z}$, where $\boldsymbol{\rho} = x\boldsymbol{x} + y\boldsymbol{y}$ is the transverse coordinate with respect to z.

When a plane pulse wave irradiates upon a semiinfinite random media, the two-frequency mutual coherence function can be obtained by solving the following equation:[15]

$$\left[\frac{\partial}{\partial\eta} + \frac{{\rm i}k_{\rm d}z}{2k_1k_2}\nabla_{\rm d}^2 - {\rm i}K_1z - ({\rm i}K_2)^*z - P(\boldsymbol{\rho}_{\rm d})z\right]\Gamma = 0. \tag{12}$$

For most practical situations, the pulse bandwidth is smaller than the carrier frequency, and the sizes of particles are larger than a wavelength. Using the two approximations, the two-frequency mutual coherence function[15] is given by

$$\Gamma = A(\omega_{\rm d})\exp[{\rm i}\phi(\omega_{\rm d}) + {\rm i}(\omega_{\rm d}/v_{\rm p})z], \tag{13}$$

$$A(\omega_{\rm d}) = \exp\{-\rho\sigma_{\rm t}z[1-(W_0/x)\tan^{-1}x]\}, \tag{14}$$

$$|\Gamma_1(\omega_{\rm d})| = \exp\left[-\tau\left(1-x\tan^{-1}x\right)\right], \tag{15}$$

$$\phi(\omega_{\rm d}) = (\rho\sigma_{\rm t}z)[(W_0/x)\ln(1+x^2)], \tag{16}$$

where the dimensionless parameter x is expressed as $x = \omega_{\rm d}/\omega_{\rm r}$, $\omega_{\rm r} = 2\gamma v_{\rm p}/z$ is a characteristic angular frequency, $W_0 = \sigma_{\rm s}/\sigma_{\rm t}$ is albedo of a single aggregate, $\sigma_{\rm t}$ is the extinction cross section, $\sigma_{\rm s}$ is the scattering cross section, $\omega_{\rm d}$ is frequency difference, $v_{\rm p}$ is the phase velocity, and z is the propagation distance of pulses.

3. Numerical results of scattering characteristics of soot aggregates by GMM

In this section, the scattering characteristics of soot aggregates are calculated and discussed. The results obtained here will be applied to the pulse propagation in soot aggregate systems.

Based on the DLA model, the soot aggregates are simulated in Figs. 2(a) and 3(a). The relationship between the fractal dimension and the monomer number is expressed by the equation $N = k_g(R_g/r_p)^{D_f}$, where N is the monomer number, R_g is the cyclotron radius, r_p is the radius of a monomer, $k_g = 1.27$ is the forward factor, and D_f is the fractal dimension. In Fig. 2(a) the radius of a spherical monomer is 100 μm, while in Fig. 3(a) is 85 μm. When the incident plane wave vector is along the positive z direction in the coordinate system, the distributions of scattering intensities for three different cases are displayed in Figs. 2(b) and 3(b). The numbers of azimuth angles in the range of (0, 360) degrees for three cases are 40, 20, and one, respectively. As shown in Figs. 2(b) and 3(b), the scattering intensities of case 1 are very close to those of case 2, but are very different with those of case 3. These results indicate that the orientation of aggregates is closely related to the distributions of scattering intensities.

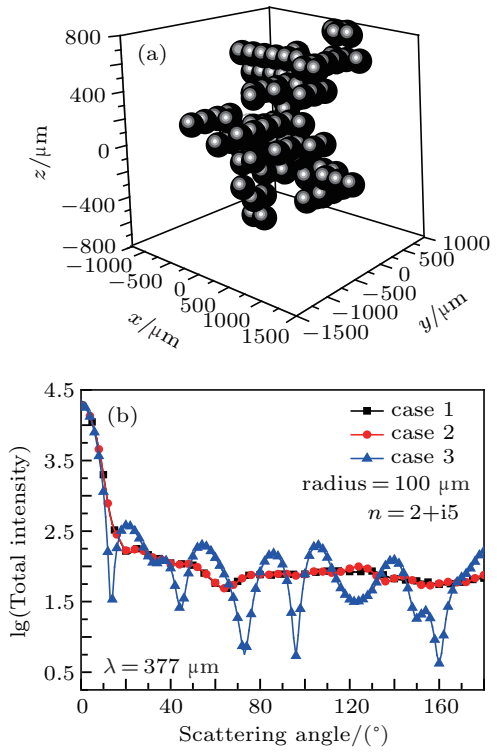


Fig. 2. (color online) Soot aggregates model consisting of 100 spheres and distribution of scattering intensities. (a) The radius of a monomer is 100 μm. (b) The distribution of scattering intensities for three cases.

Tables 1 and 2 show the scattering parameters including scattering cross sections, extinction cross sections, and absorption cross sections for the three cases. It appears that the orientation of aggregates has little effect on these cross sections. With these parameters, we can further analyze pulse propagation in soot aggregate systems.

A soot aggregate with 200 spheres is shown in Fig. 4(a). The fractal dimensions D_f of the three aggregates are 2.12, 2.01, and 2.09, respectively. The differences among them are small, however, the forward scattering intensity of Fig. 4(a) is larger than those of Figs. 2(a) and 3(a). The effects of the number and radius of the monomer on the scattering intensities of system may be more obvious than that of fractal dimension.

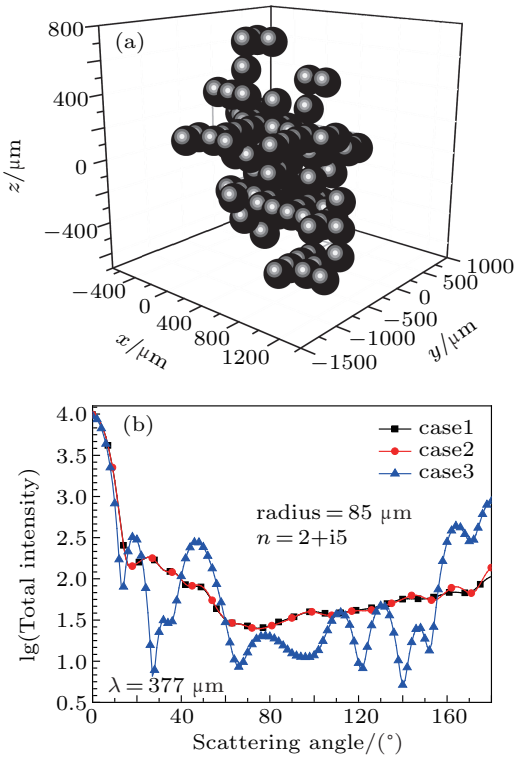


Fig. 3. (color online) Soot aggregates model consisting of 100 spheres and distribution of scattering intensities. (a) The radius of a monomer is 85 μm. (b) The distribution of scattering intensities for three cases.

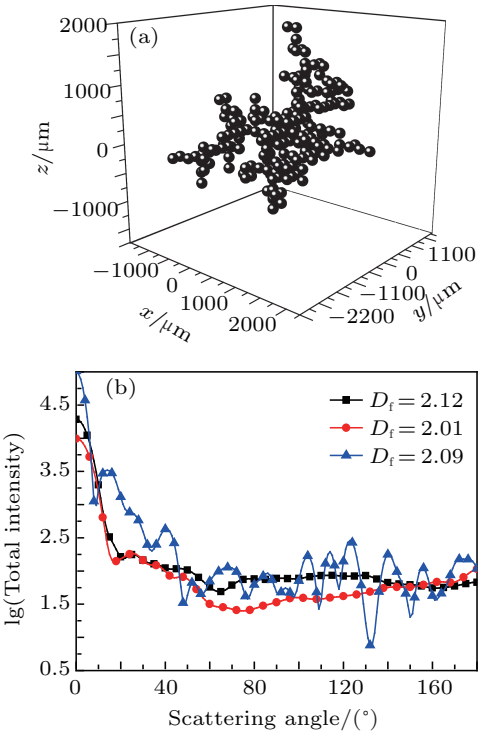


Fig. 4. (color online) Soot aggregates model consisting of 200 spheres and comparison of scattering intensities. (a) The radius of a monomer is 100 μm. (b) A comparison of scattering intensities among three models.

Table 1. Scattering parameters of the model in Fig. 2 (the frequency of the incident wave is 0.7956 THz).

	σ_t	σ_a	σ_s
Single orientation	4.4461×10^6	1.6447×10^6	2.8009×10^6
Average value for 20 orientations	4.4137×10^6	1.4943×10^6	2.9187×10^6
Average value for 40 orientations	4.4128×10^6	1.4906×10^6	2.9214×10^6

Table 2. Scattering parameters of the model in Fig. 3 (the frequency of the incident wave is 0.7956 THz).

	σ_t	σ_a	σ_s
Single orientation	3.1014×10^6	1.0950×10^6	2.0060×10^6
Average value for 20 orientations	3.1542×10^6	1.0270×10^6	2.1267×10^6
Average value for 40 orientations	3.1555×10^6	1.0259×10^6	2.1291×10^6

4. Numerical results of pulse propagation characteristics by using two-frequency mutual coherence functions

In this section, the THz pulse propagation properties in soot aggregate systems are described by the two-frequency mutual coherence function. The variations of normalized amplitude and phase versus the optical distance τ_t are shown in Figs. 5 and 6. The optical distance τ_t is the product of number density ρ, extinction cross section σ_t and the propagation distance z. In our results, the number density and extinction cross section are constant, in other words, the x-axis coordinate can be regarded as z. The center frequency of pulse is 0.7956 THz. The pulse bandwidth is 20 GHz. The refractive index $n = 2 + i5$ and is shown in the figures.

The scattering characteristics of a single aggregate can have an important influence on pulse propagation analysis. In Fig. 5, four different cases are considered for the soot aggregate model in Fig. 3(a). The differences between the normalized amplitudes among the four cases are very small. However, the phase for the surface-equivalent sphere case is far less than those for the other three cases. Figure 6 gives the normalized amplitude and phase of the two-frequency mutual coherence function for the model in Fig. 2(a). The normalized amplitude of case 1 is coincident with that of case 3. For the same optical distance, the normalized amplitudes of case 1 and case 3 are smaller than that of case 2, and the phase of case 1 is smaller than those of case 2 and case 3. As the optical distance τ_t increases, the normalized amplitude decreases gradually.

The relevance of two waves with different frequencies at the same time and the same position can be described by the coherent bandwidth. Here, one factor[15] α is introduced as

$$\alpha = \frac{|\Gamma_1(\omega_d)| - \exp(-\tau/W_0)}{|\Gamma_1(\omega_d = 0)| - \exp(-\tau/W_0)}, \tag{17}$$

where α is the normalized solution of $|\Gamma_1|$. Generally, the coherent bandwidth is defined as the frequency difference f_d at which $\alpha = 0.5$. The variations of α versus x are shown in Fig. 7. As the optical increasing, the dimensionless parameter x is decreasing at which $\alpha = 0.5$.

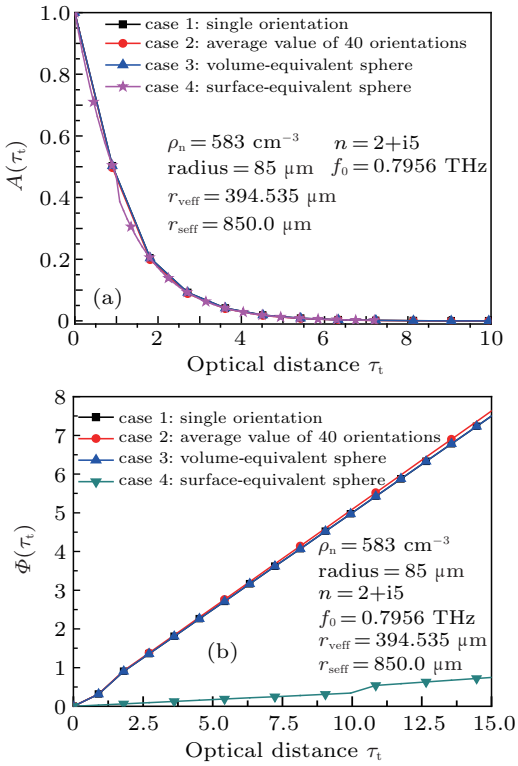


Fig. 5. (color online) Variation of two-frequency mutual coherence function for the soot aggregate model in Fig. 3(a): (a) $A(\tau_t)$ and (b) $\Phi(\tau_t)$.

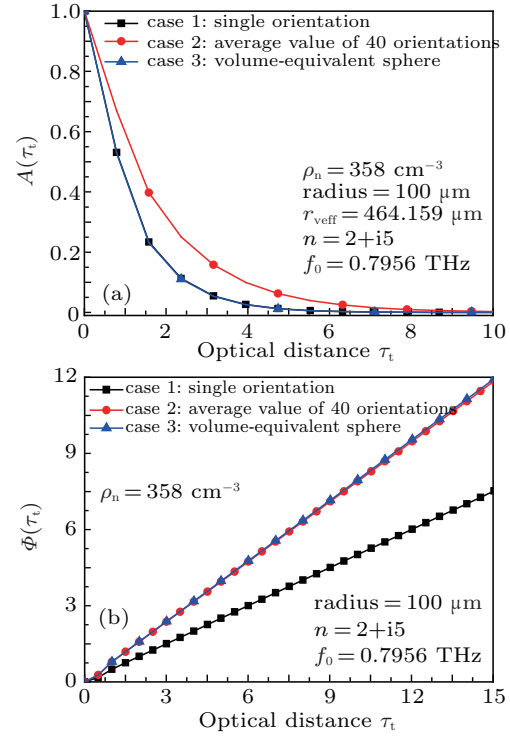


Fig. 6. (color online) Variation of two-frequency mutual coherence function for the soot aggregate model in Fig. 2(a): (a) $A(\tau_t)$ and (b) $\Phi(\tau_t)$.

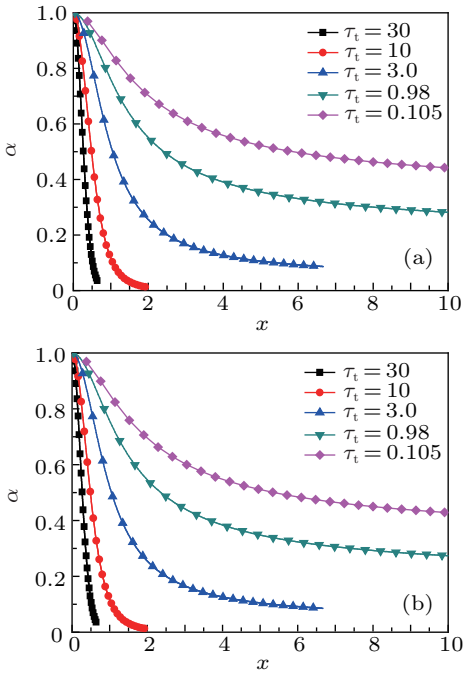


Fig. 7. (color online) Variation of α as a function of x and the optical distance τ_t. (a) The single orientation of the soot aggregate model in Fig. 2(a) and (b) the single orientation of the soot aggregate model in Fig. 3(a).

The parameter x is in relation with the frequency difference f_d. Therefore, with the definition of x given in Section 2, we can obtain the coherent bandwidth f_d for any optical distance. The variation of x as a function of optical distance is shown in Fig. 8.

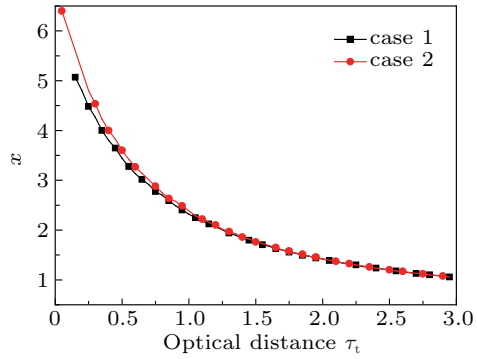


Fig. 8. (color online) Variation of x as a function of optical distance at $\alpha = 0.5$. (a) Case 1: the model in Fig. 3(a) and (b) case 2: the model in Fig. 2(a).

5. Conclusions

In this paper, scattering characteristics of different kinds of soot aggregates in a THz wave are studied in detail. The effects of azimuth angle rotation on scattering intensities are obvious, while their effects on cross sections are less so. Considering a random soot aggregate system, the two-frequency mutual coherence functions of a plane pulse are presented. A conclusion that the different equivalent methods have great effects on the normalized amplitudes and phases is obtained. The coherent bandwidth is analyzed by the dimensionless factor x. Our results will provide some important theoretical basis for research on atmosphere environment detection and THz wave communication techniques.

References

[1] Sorensen C M, Cai J and Lu N 1992 *Appl. Opt.* **31** 6547
[2] Witten Jr T A and Sander L M 1981 *Phys. Rev. Lett.* **47** 1400
[3] Dragoman D and Dragoman M 2004 *Prog. Quant. Electron.* **28** 1
[4] Pickwell E, Cole B E, Fitzgerald J A, Wallace V and Pepper M P 2004 *Appl. Phys. Lett.* **84** 2190
[5] Purcell E M and Pennypacker C R 1973 *Astrophys. J.* **186** 705
[6] Waterman P C 1971 *Phys. Rev. D* **3** 825
[7] Chew W C 1995 *IEEE Trans. Antenn. Propag.* **43** 1483
[8] Gouesbet G, Grehan G and Maheu B 1983 *Appl. Opt.* **22** 2038
[9] Xu Y L and Gustafson B A S 2001 *J. Quant. Spectrosc. Radiat. Transf.* **70** 395
[10] Huang C J, Liu Y F and Wu Z S 2007 *Acta Phys. Sin.* **56** 4068 (in Chinese)
[11] Li H Y, Wu Z S and Bai L 2010 *J. Electromagnet. Wave* **24** 2037
[12] Knollman G C 1965 *J. Appl. Phys.* **36** 3704
[13] Ishimaru A and Hong S 1975 *Radio Sci.* **10** 637
[14] Hong S and Ishimaru A 1976 *Radio Sci.* **11** 551
[15] Hong S, Sreenkivasiah I and Ishimaru A 1977 *IEEE Trans. Antenn. Propag.* **25** 822
[16] Kuga Y, Ishimaru A, and Bruckner A P 1983 *J. Opt. Soc. Am.* **73** 1812
[17] Sreenkivasiah I and Ishimaru A 1979 *Appl. Opt.* **18** 1613
[18] Young C Y, Ishimaru A and Andrews L C 1996 *Appl. Opt.* **35** 6522
[19] Liu W J, Mao H Y, Fu G Q and Qu S L 2010 *Acta Phys. Sin.* **59** 913 (in Chinese)
[20] Huang C J, Liu Y F, Wu Z S, Sun Y Q and Long S M 2009 *Acta Phys. Sin.* **58** 2397 (in Chinese)
[21] Lei C X, Zhang H F and Liu H F 2009 *Acta Phys. Sin.* **58** 7168 (in Chinese)
[22] Li H Y, Wu Z S and Li Z J 2010 *Proc. SPIE* 7854 *Infrared, Millimeter Wave, and Terahertz Technologies*, November 15, 2010, Beijing, China, p. 785419